Haider, MHA.; Nasir, S.; Ali, M.; Ramirez Hoyos, P.; Cervera, J.; Mafe, S.; Ensinger, W. (2022). Osmotic energy harvesting with soft-etched nanoporous polyimide membranes. Materials Today. 23:1-10. https://doi.org/10.1016/j.mtener.2021.100909

Osmotic Energy Harvesting with Soft-Etched Nanoporous Polyimide Membranes

M. Hamza Ali Haider[a,#], Saima Nasir[a,b,#], Mubarak Ali[a,b,*], Patricio Ramirez[c], Javier Cervera[d], Salvador Mafe[d], and Wolfgang Ensinger[a]

[a]*Department of Material- and Geo-Sciences, Materials Analysis, Technische Universität Darmstadt, Alarich-Weiss-Str. 02, D-64287 Darmstadt, Germany*

[b]*Materials Research Department, GSI Helmholtzzentrum für Schwerionenforschung, Planckstr. 1, D-64291, Darmstadt, Germany*

[c]*Departament de Física Aplicada. Univ. Politècnica de València. E-46022 Valencia, Spain*

[d]*Departament de Física de la Terra i Termodinàmica, Universitat de València, E-46100 Burjassot, Spain*

# Equal contributions

*Corresponding author:

Email address: m.ali@gsi.de

Abstract

We present the study of osmotic energy harvesting with soft-etched nanoporous polyimide membranes for a wide range of salt concentration differences, ion irradiation fluences, and multipore orientations (parallel or network). The effect of solution pH and divalent cations on the membrane performance is also investigated. The membrane behavior is evaluated in terms of the reversal potential (V_{rev}), the maximum power generation (P_{max}), and the energy conversion efficiency (η_{max}). For an exposed membrane area of ~1 cm^2, the maximum values obtained for these parameters are V_{rev} = 123 mV, P_{max} = 0.45 μW, and η_{max} = 40%, respectively. A significant decrease in the membrane performance is observed for membrane samples obtained with ion fluences higher than 4×10^9 ions cm^{-2} because of pore overlapping and the diffusional resistance of the external solution boundary layers at very low ionic concentrations. The soft-etched membranes are able to hold the reversal potential for several days.

Keywords: Soft-etching, heavy ion irradiation, polyimide membranes, energy harvesting, reverse electrodialysis, nanopores

1. Introduction

Increasing environmental concerns have prompted the exploration of alternative energies based on the conversion of ambient energy into electrical energy [1, 2]. Mechanical, temperature gradient, pressure gradient, salinity gradient, wind, and solar conversion mechanisms have been explored [3-8]. Reverse electrodialysis (RED) allows the generation of electricity from a salinity gradient [9] by converting the Gibbs free energy of mixing into electrical energy [2]. The RED setup is based on high and low concentrated salt solutions separated by an ion exchange membrane [10] that preferentially transports counterions and restricts the transport of coions [1, 11]. This selective transport eventually establishes an electrical potential difference in combination with the redox reactions occurring at the electrodes [1]. Two main factors affect the membrane performance: the counterion selectivity and the resistance to ionic flow [12]. The selectivity is controlled by the fixed charge concentration and average radii of the membrane pores [13].

Polyimide (PI) foils are used for many applications because of their mechanical, chemical, and thermal stability [14]. Porous PI membranes are fabricated through chemical track etching and the multiple solvent displacement method, curing the polymer solution on a nanoporous template [15-19]. The conventional track-etching utilizes an inorganic etchant such as a sodium hypochlorite (NaOCl) solution for the fabrication of porous structure [20, 21]. The method requires harsh conditions and subnanometer pores are difficult to obtain. Recently, a soft etching method was reported by Ensinger and coworkers using organic solvents in heavy ion irradiated PI membranes [17-19]. In the usual chemical track-etching, the inorganic etchant breaks the imide bond in the PI membrane whereas in the soft-etch method the organic solvents only dissolve the damaged trails inside the tracks for the fabrication of the nanopores without affecting the bulk material [17, 18]. Previously, Wang *et al.* have obtained subnanometer sized pores in polyethylene terephthalate (PET) membranes by irradiation with an UV beam for a long period of time [22]. Also, Lu *et al.* have fabricated a subnanometer porous membrane by growing metal organic frame works inside the porous PET template [23].

Membranes with high counterion selectivity and low resistance to ionic current are suitable for the conversion of electrical energy. Experimental [8, 24, 25] and theoretical [26-28] studies show that a charged nanoscale pore having a diameter comparable to the Debye length generates significant diffusion potential (E_{diff}) and zero-voltage current (I_0) values when exposed to a concentration gradient. Kwon *et al.* have demonstrated that noticeable E_{diff} and I_o values can be obtained from

track etched polycarbonate membranes exposed to a concentration gradient [1]. Laucirica *et al.* have reported the generation of electrical power from a bullet-shaped nanochannel in a PET membrane [12]. Balme *et al.* have also demonstrated energy harvesting from a PET conical nanopore membrane functionalized with chitosan/polyacrylic acid multilayers and hydrogels. The nanopores were obtained from the chemical etching of latent tracks in the polymeric membrane [29].

In our case, the PI membranes with subnanometer pores were fabricated by the soft etching technique using anhydrous dimethylformamide (DMF) as an organic solvent. The membrane generated significant E_{diff} and I_0 values when exposed to a concentration gradient due to the small pore radii and negative surface charges. The values of E_{diff} and I_0 were used as benchmarks for comparing the membrane performance obtained with different experimental conditions concerning the irradiation fluence, parallel and network array multipore geometries, and mono and divalent cation solutions for a wide range of concentration gradients and pH values. The stability of the RED setup was studied for a 15-day time period.

2. Materials and methods

The polyimide (PI) foils of thickness ~13 μm (DuPont™ Kapton® HN) were irradiated by a swift heavy metal ion (Au^{26+}) beam of energy 11.4 MeV per nucleon. The angle of the beam with respect to the sample surface was 90° or 45°. With this setup, the PI samples were irradiated with different fluences: 4×10^8, 8×10^8, 4×10^9, 8×10^9, and 4×10^{10} ions cm^{-2}. The ion beams caused the irreversible damage of the PI membranes, leading to the formation of latent ion tracks. The PI foils were further sensitized by UV rays of wavelength 320 nm on each side for 1 h.

The membrane pores were obtained using the soft-etching technique [17-19] by soaking the samples in the DMF solvent for ~24 h at room temperature (see Figure S1). After etching, the PI foils were washed, first with ethanol and then three times with distilled water.

The functional groups on the pore surface undergo protonation and deprotonation reactions depending of the pH of the electrolyte solution. Note in particular that the carboxylate moieties are deprotonated (ionized) at high pH values because typical *p*Ka values of these chemical groups is in the pH range 4 - 6. Therefore, the ionized carboxylate moieties act as negative fixed charges on

the pore surface under physiological conditions. Under acidic conditions, these moieties are neutral due to protonation. This fact influences the surface charge and the membrane output performance.

The membrane sample was fixed in between the two compartments of a home-made conductivity cell. The membrane area exposed to the electrolyte solutions was 1.1 cm^2. The aqueous electrolyte solution (0.1 M NaCl) was filled in both cell compartments and Ag/AgCl electrodes were immersed in the solutions. To further remove the damaged material from the soft-etched pores, a triangular wave signal was applied, with an amplitude voltage of 2 V and a step size of 0.1 V for 30 periods. The measured currents are shown in Figure S2. The peak currents at +2 V and –2 V increase after every cycle indicating the removal of the damaged material from the pores. This process was terminated when the ion current was approximately stable. After washing several times with deionized water, the compartments were refilled with different KCl concentrations in order to establish a concentration gradient. All electrolyte solutions were prepared in deionized water with pH values in the range 5.8 – 6.3. The reversal potential $V_{rev} = E_{diff}$ corresponding to the zero current condition [25] and the ion current at zero potential (I_0) were obtained using a Keithley multimeter 6487 and a Faraday's cage, with a triangular wave signal of potential amplitude from –60 mV to 140 mV and a scan rate of 4 mV s^{-1}, for three periods.

The experimental setup is shown in Figure 1(a). Most experiments were conducted at room temperature using three different membrane samples. The resulting error bars obtained with these samples, not with three different cycles, are shown for each experimental point. Also, the membrane performance was studied over a 15-day time period for different multipore geometries, exposition fluences, and salt conditions.

3. Results and Discussion

The soft-etched (SE)-PI membrane has nanometer pores that are negatively charged, as evidenced by the selective transport of monovalent cations and the limited transport of divalent cations, alkylammonium cations, metal-crown chelates, and solvated metal ions across the membranes [17-19]. However, while we have attempted to obtain clear pore images, the fact is that the FESEM imaging of the pores in the polymeric membrane is exceedingly difficult here because charging of the sample can deflect the scanning beam. Thus, we resorted to the analysis of the transport of quaternary ammonium ions and crown-ether cations, studying their corresponding current drops

[18]. For instance, Pr_4N^+ (effective size ~0.9 nm) and Bu_4N^+ (~1.0 nm) and the metal-crown chelates $[Na(15C5)]^+$ (~0.81 nm) and $[K(18C6)]^+$ (~1.15 nm) virtually blocked the channels, suggesting that their nanoscale sizes are commensurate with the channel opening diameter.

These above pore characteristics are suitable for the conversion of osmotic energy into electrical energy under salinity gradient conditions. To this end, the high KCl solution concentration in the left compartment of the cell is kept constant at three different values C_H = 0.1, 0.5 and 1 M. The low concentration (C_L) in the right compartment is gradually increased from 1 – 50 mM, 1 – 100 mM and 1– 500 mM for the above fixed concentrations C_H = 0.1, 0.5 and 1M, respectively (Figure 1a). In this way, the value of concentration ratio (C_H/C_L) decreases from 100 to 2, from 500 to 5, and from 1000 to 2, respectively, as shown in Figure 2. Ag/AgCl electrodes with 3 M KCl salt bridges are immersed on each solution side of the membrane (see the section *Correction associated with the use of salt bridges* in the *Supporting Information* where this technique is theoretically justified in our case). A voltage is applied across the membrane to obtain the *I–V* characteristics and the reversal potential $V_{rev} = E_{diff}$ is measured from the zero current condition (Figure 1b).

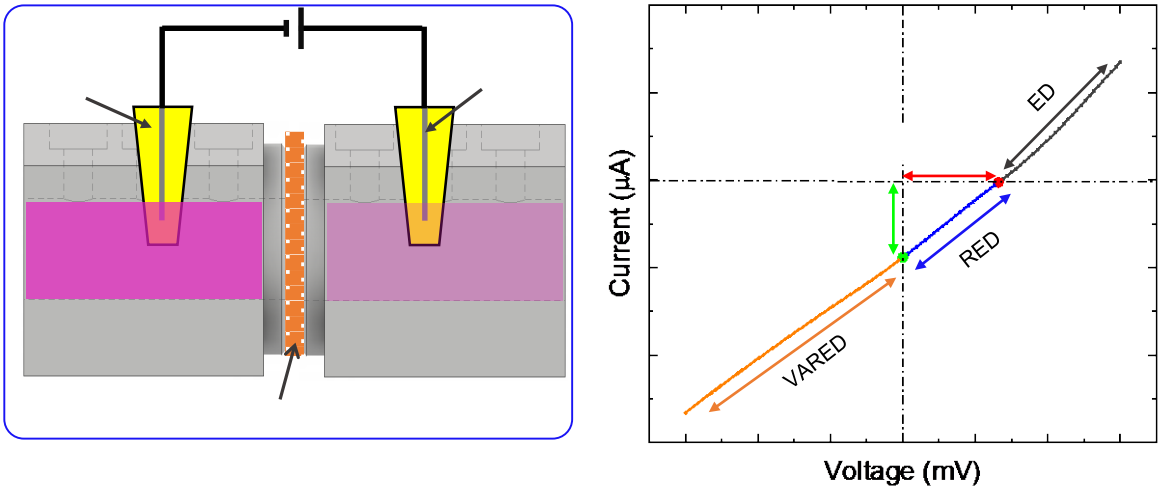

Figure 1. (a) Scheme of the energy harvesting setup. (b) Schematic *I–V* curve representing the electrical magnitudes and ion transport regimes obtained under the applied concentration gradient.

Figure 1(b) schematically shows the *I–V* curve and the different ionic transport regimes. The positive current $I > 0$ at $V > 0$ corresponds to the electrodialysis (ED) regime where the applied

electric field acts against the concentration gradient and has a dominant role on the cation transport compared to that of diffusion. Hence, the cations are electrically conducted against the concentration gradient. The ED regime is normally used in water desalination applications. The red circle intercept at the x-axis gives the diffusion potential (E_{diff}). Note that E_{diff} is the reversal potential (V_{rev}) at which the ionic current across the membrane is zero (Figure 1b) because ionic conduction exactly compensates for diffusion in this case.

The blue region of the I–V curve with negative currents $I < 0$ at $V > 0$ constitutes the reverse electrodialysis (RED) regime where the cation diffuses down the concentration gradient. In the RED regime the role of the electric conduction is decreased compared with that of diffusion. The green circle intercept at the y-axis gives the ion current (I_0) at zero voltage where the cations move down the concentration gradient exclusively. The orange region at $V < 0$, represents the voltage-assisted reverse electrodialysis (VARED) regime where the cation transport is due to both diffusion and electric conduction. The RED region permits to obtain the cation transference number (t_+) from the value of V_{rev}. The maximum power is obtained in terms of I_0 and V_{rev} (Figures 2 – 6).

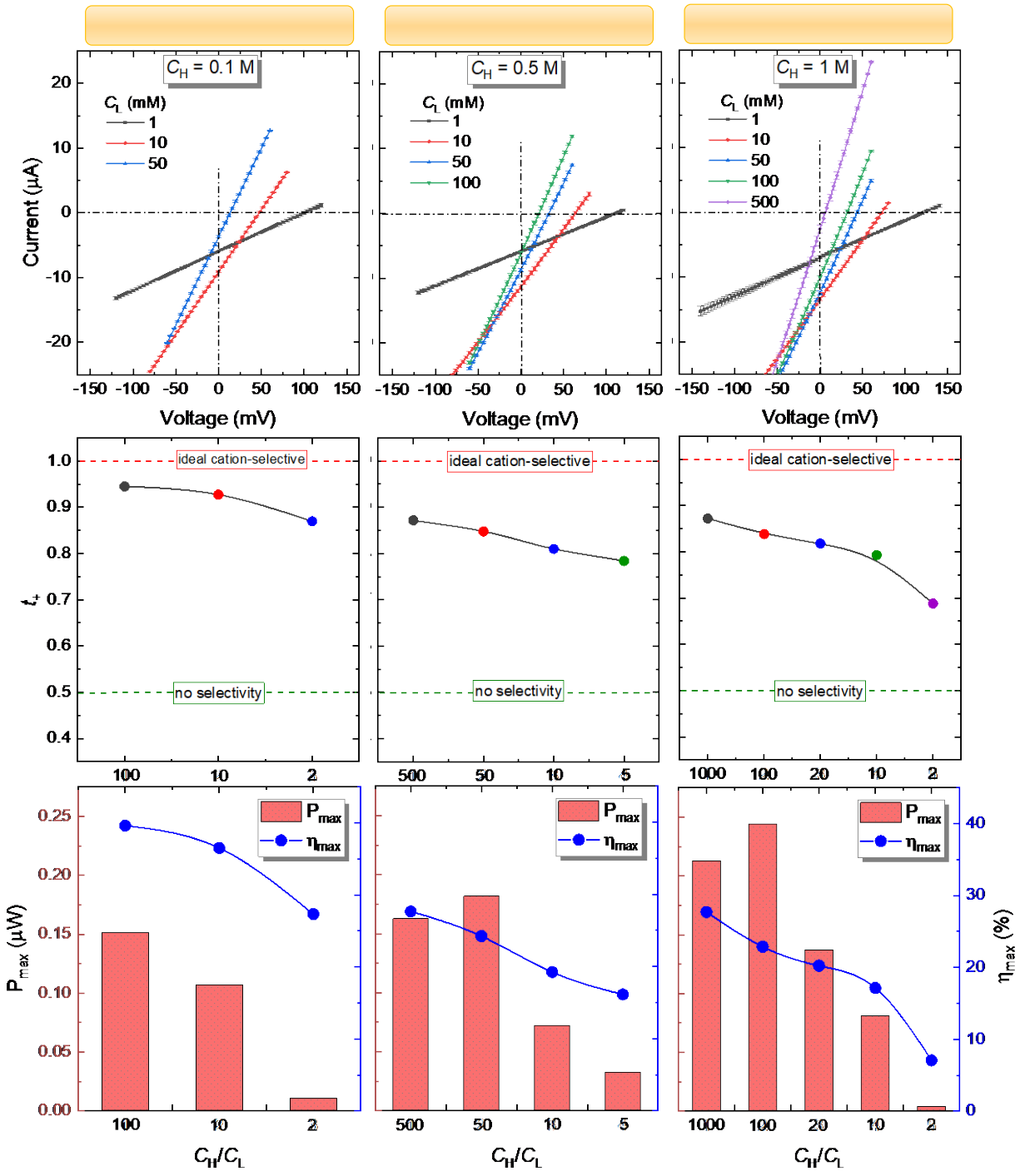

Figure 2. The effect of the KCl concentration ratio on: (a) the *I–V* characteristics, (b) the cation transference number, and (c) the maximum power generation and energy conversion efficiency for a SE-PI membrane with 8×10^8 pores cm^{-2}. Note that the absolute values of the current depend on the sign of the applied voltage *V* with respect to that of the concentration difference $C_H - C_L > 0$ in Figure 1(a).

Figures 2a (i–iii) show that V_{rev} decreases by increasing the lower concentration (C_L) for each fixed high concentration (C_H = 0.1, 0.5 or 1M). Note that I_0 first increases by increasing C_L from 1 to 10 mM and then decreases by further increase in C_L in the membrane with 8×10^8 pores cm^{-2}, thus emphasizing the dominant role of diffusion over electric conduction in the RED regime. As expected, Figure 2a(i-iii) shows that the highest values V_{rev} = 100, 111, and 123 mV and the corresponding currents at zero potential, I_0 = 6.0, 5.8, and 7.0 μA are obtained in the cases C_H/C_L = 100 (0.1 M|1 mM), 500 (0.5 M|1 mM) and 1000 (1 M|1 mM), respectively. The cation transference number (t_+) of Figure 2(b) gives the cation selectivity: t_+ approaches 1 for an ideally cation selective membrane while it is close to 0.5 for a non-selective membrane. The values of t_+, the maximum power generation (P_{max}) and the energy efficiency (η_{max}) can be calculated from equations 1-3 below, where R is the gas constant, T is the temperature, F is the Faraday constant, and a_H and a_L are the activities of the solutions [12]:

$$t_+ = \frac{1}{2}\left[1 + \frac{F}{RT}\frac{E_{diff}}{\ln(\frac{a_H}{a_L})}\right] \qquad (1)$$

$$P_{max} = \frac{E_{diff} I_o}{4} \qquad (2)$$

$$\eta_{max} = 100\frac{(2t_+ - 1)^2}{2} \qquad (3)$$

The activity values were taken from the electrochemical literature [30, 31]. Figure 2(b) shows that the cation transference number t_+ is decreased by decreasing C_H/C_L because of the increasing salt concentrations. Figure 2(c) shows the maximum power generation and energy efficiency values obtained at different C_H/C_L ratios from equations 2 and 3, respectively [12]. The value of P_{max} decreases from 0.15 to 0.01 μW by decreasing C_H/C_L from 100 to 2 in the case of the concentration gradient 0.1 M|1–50 mM for a membrane with 8×10^8 pores cm^{-2} and an exposure area of ~1 cm^2. Under these conditions, the highest obtained values of P_{max} for C_H/C_L = 50 (0.5 M|10 mM) and 100 (1 M|10 mM) are 0.18 and 0.25 μW, respectively, as shown in Figure 2c (ii and iii). Moreover, the highest η_{max} values 40 and 37 are obtained for the cases C_H/C_L = 100 (0.1 M|1 mM) and 10 (0.1 M|10 mM). For the rest of the concentration differences, η_{max} varies from 7 to 28, as shown in Figure 2(c).

We have also conducted additional experiments aimed at comparing the performance of different SE-PI membrane samples irradiated with fluences in the range 4×10^8 to 4×10^{10} ions cm^{-2} under different concentration gradients (Figure 3). Figure 3a (i-iv) shows that the fluences 4×10^8, 8×10^8, and 4×10^9 ions cm^{-2} generated an approximately constant V_{rev} value, even at different C_H/C_L ratios. However, a decrease in V_{rev} is observed for fluences higher than 4×10^9 ions cm^{-2}. Note also that I_0 also increases with the fluence, except for the case of 4×10^{10} ions cm^{-2} (Figure 3a). The values of V_{rev} and I_0 are obtained from the corresponding I–V curves of Figure S3. This decrease could be due to the overlapping of the pores at fluences greater than 4×10^9 ions cm^{-2}. Note that while the total pore area with respect to the membrane surface area is low, because of the small pore radii, the membrane thickness is relatively high. Thus, pore overlapping cannot be discarded because of the random bombardment of heavy ions during membrane irradiation process. Note that ion fluence (ions cm^{-2}) depends on the flux (ions cm^{-2} s^{-1}) of the heavy ion beam. During irradiation several bunches of heavy ion beam are bombarded on the membrane surface to reach a specified ion fluence. Therefore, for higher ion fluences the probability of ion track overlapping is not negligible.

Similarly, a drop in the cation transference number t_+ is also observed for these fluences, as shown in Figure 3(b). This result may suggest an overlapping of the membrane pores. A similar trend is observed for P_{max}, with a maximum value of 0.45 μW obtained at a fluency of 4×10^9 ions cm^{-2} and C_H/C_L =100. As to η_{max}, it decreases with increasing fluences except for a fluence of 4×10^9 ions cm^{-2}. Guo, Jiang and co-workers have recently explained with detail the experimental gap that exists between single-pore- and membrane-based nanofluidic osmotic power generators [32, 33]. In particular, they have shown clearly that the usual linear scaling gives significant deviations from the actual experimental values, in qualitative agreement with our results concerning high pore density membranes where both pore overlapping and the diffusional resistance of the external solution boundary layers can be significant. See also two recent reviews [34, 35] on nanofluidics-based osmotic energy conversion and references therein.

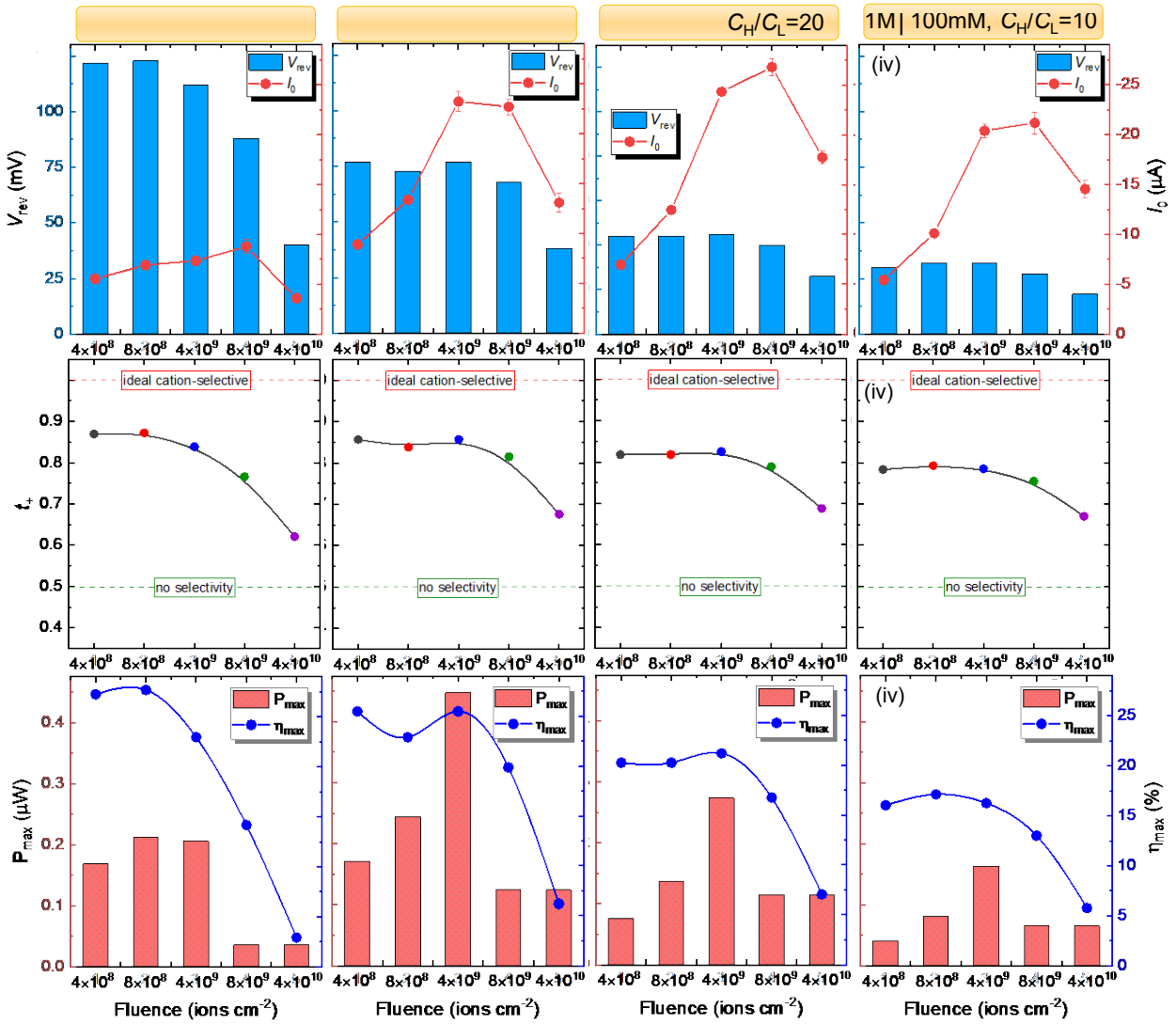

Figure 3. The effect of ion fluence on: (a) the reversal potential and ion current at zero voltage, (b) the cation transference number, and (c) the maximum power generation and energy conversion efficiency. The results are obtained for a KCl solution at different concentration ratios.

We have also checked the capability of the SE-PI membrane to hold the reversal potential for a long time period. To this end, a membrane with an ion fluence of 4×10^8 ions cm^{-2} was monitored for a period of 15 days. Although we initially fixed C_H/C_L = 100 (1 M|10 mM), the diffusion of the ions down this high concentration gradient should eventually give a lower effective value of C_H/C_L because of the time dependent concentration polarization developed at the two diffusion boundary layers flanking the membrane at low ionic concentrations. Indeed, the resulting time dependent I–V curves of Figure S5 show that V_{rev} decreases and I_0 increases with time, as indicated in Figure 4(a).

By the end of the 15th day, the membrane shows a potential of 61 mV while this potential was 94 mV initially. Note that after long term use, changes in the concentration polarization of the surrounding electrolytes can also occur, leading to changes in the V_{rev} and I_0 values with time, as can be seen in Figure 2. These relatively low values of V_{rev} may suggest a decrease in the cation selectivity with time. On the contrary, an increase of I_0 with time (Figure 4a) may be due to a decrease in the total system resistance because of the above mentioned changes. Figure 4(b) shows also that the P_{max} almost remained constant till 10th day (0.328 ±0.011 μW) and then started to decrease due to further decrease in V_{rev} and I_0 with time.

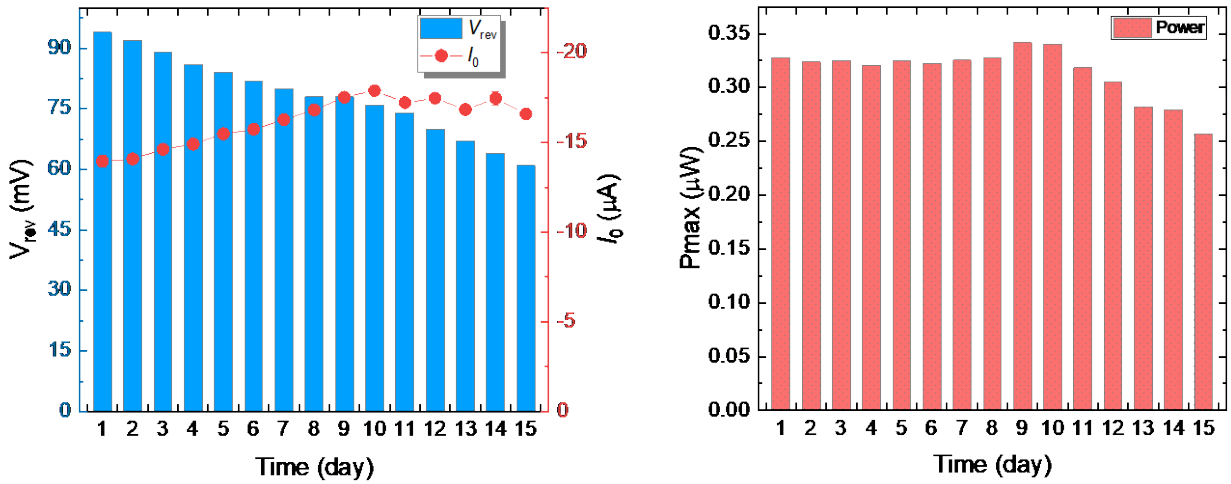

Figure 4. The time dependent changes of: (a) the reversal potential and ion current at zero voltage and (b) the maximum power generation for a SE- PI membrane obtained with the fluence 4×10^8 pores cm^{-2}. The results correspond to a KCl solution with the concentration ratio 1 M|10 mM.

Figure 5 shows the performance of the SE-PI membranes at close to neutral (pH = 6.3) and acidic solutions (pH = 3.0). At pH = 6.3, the membrane shows higher V_{rev} and I_0 values compared with those of acidic conditions (Figure 5a). The values of V_{rev} and I_0 are obtained from the corresponding *I–V* curves of Figure S4. Moreover, at pH = 3.0 the cation transference number t_+ remained almost constant, between 0.57 and 0.6, suggesting the loss of the membrane cation selectivity under acidic conditions. On the contrary, t_+ is above 0.8 at pH = 6.3, as shown in Figure 5(b). Furthermore, the membrane shows high P_{max} and η_{max} values at pH 6.3, while these parameters are close to zero at acidic pH (Figure 5c). These results reflect the different roles played by the solution pH on the cation selectivity and performance of the SE-membranes.

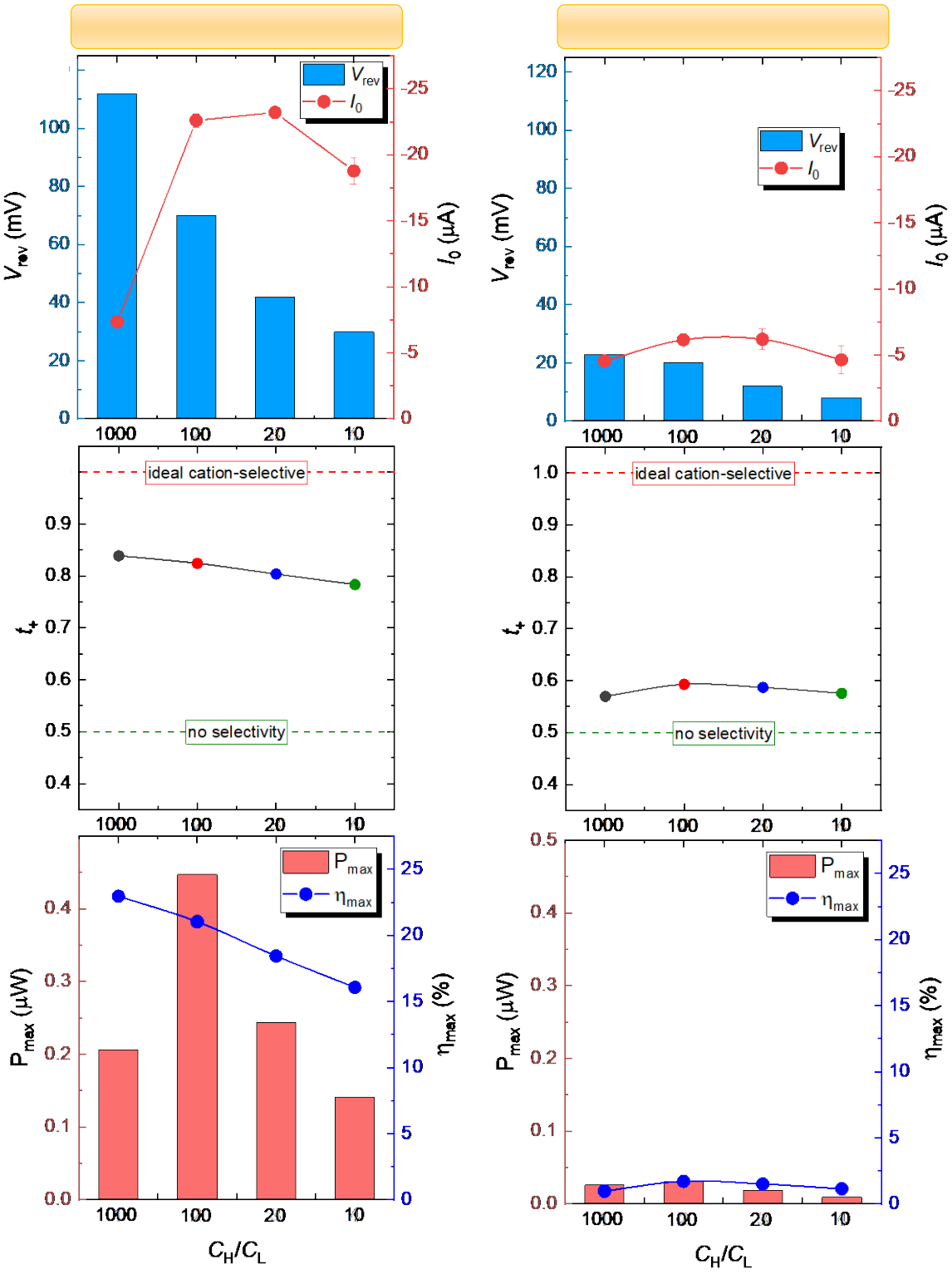

Figure 5. The solution pH dependent changes of: (a) the reversal potential and the ion current at zero voltage, (b) cation transference number and (c) the maximum power generation and energy conversion efficiency for a SE- PI membrane obtained with the fluence 4×10^9 pores cm^{-2}. The results correspond to KCl solutions of different concentration ratios at pH = 6.3 and 3.0.

Figure 6 shows the performance of the SE-PI membranes fabricated with parallel (PLPN) and network (NWNP) nanoporous structures irradiated with ion fluences of 4×10^8, 8×10^8, 4×10^9 and 4×10^9 ions cm^{-2}. The pores in the PLPN case should be approximately perpendicular to the plane surface of the membrane and thus do not cross each other to a great extent. On the contrary, the pores in the NWNP case can cross each other because they were obtained by ion irradiation at 45° angle with respect to the plane surface of the membrane from the four directions [36]. The changes in V_{rev} of membranes having the PLPN and NWNP structure are similar. On the contrary, the I_0 values of the membrane having PLPN structures are higher compared with the NWNP ones (Figure 6a). Note that the V_{rev} and I_0 values are obtained from the corresponding I–V characteristics shown in Figure S6. Also, membranes having PLPN and NWNP exhibit almost similar t_+ values (Figure 6b). Figure 6(c) shows that the PLPN membranes having fluences lower than 4×10^9 ions cm^{-2} give higher P_{max} values than those of the NWNP membranes. On the contrary, the NWNP membrane with fluences higher than 4×10^9 ions cm^{-2} give higher P_{max} values compared to PLNP membranes. Also, the η_{max} values of the PLPN membranes are higher than those of the NWNP membranes due to their relatively high V_{rev} values. These results reflect the different roles played by the nanoporous membrane structure on the cation selectivity and ionic flow resistance. The experimental data showed that at low fluences the performance of membrane having PLNP structure is better than the NWNP one in terms of the η_{max} and P_{max} values. On the contrary, the NWNP membrane exhibits higher P_{max} values compared with the PLNP one at high fluences.

Recent efforts have addressed the problem of the membrane resistance, designing composite and hybrid membranes with low internal resistances as a route to enhance the salinity gradient energy harvesting performance [37, 38]. For instance, the insertion of boron nitride (BN) nanosheets permits the internal resistance to ion transport to be reduced and the diffusion current to be increased. In addition, by varying the BN content of the resulting hybrid membrane the output current and power density can be adjusted [37]. It is also possible to decrease the resistance of ion transport, keeping a high ion selectivity, by designing composite membranes based on the assembly of graphene oxide nanosheets and cellulose nanofibers [38]. Note also that at high concentration gradients, high pore densities, and low ionic concentrations, an effectively decreased value of C_H/C_L may contribute to the total system diffusional resistance because of the time dependent

concentration polarization developed at the two diffusion boundary layers flanking the membrane [39, 40].

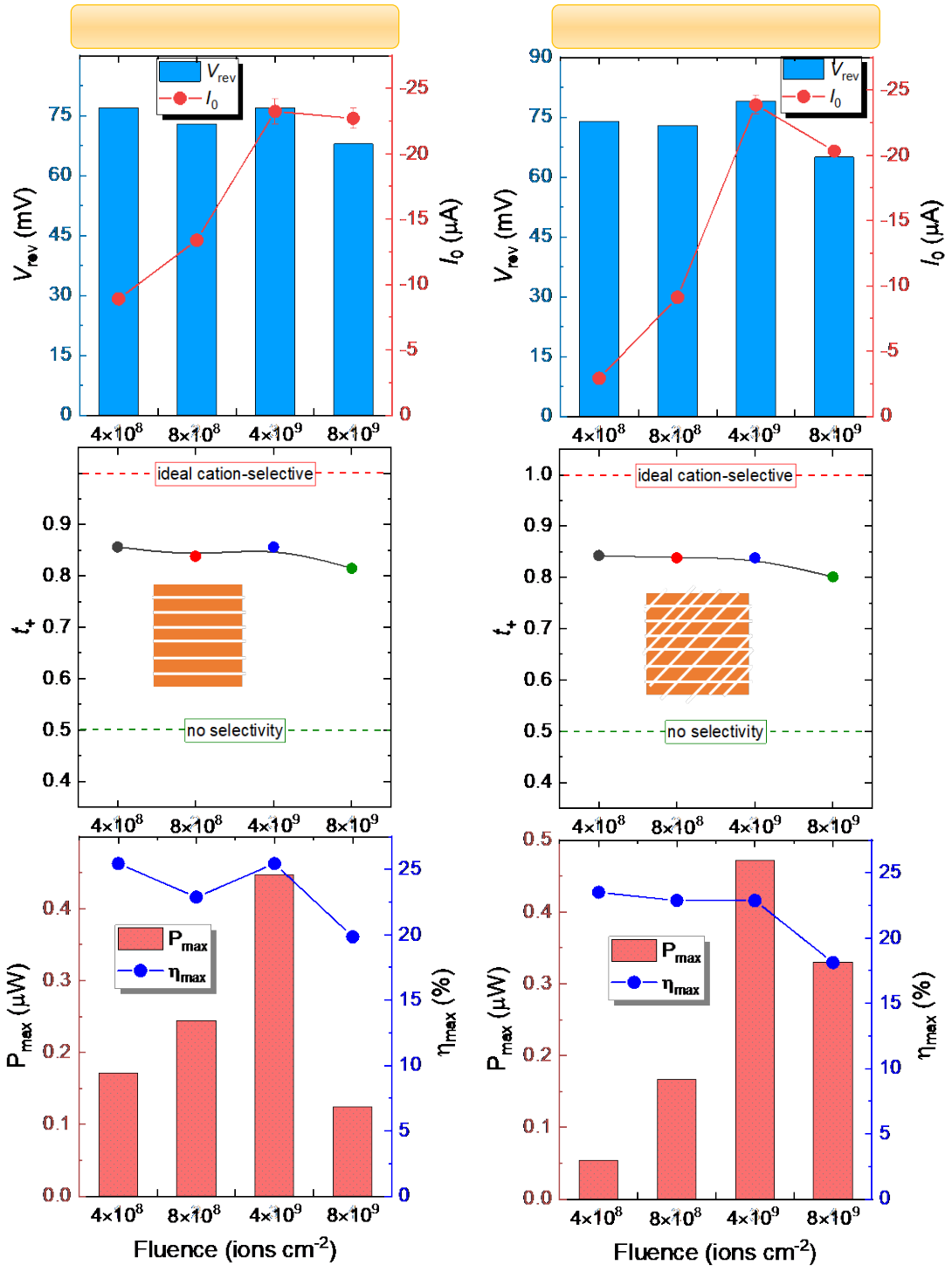

Figure 6. The effects of ion fluence on: (a) the reversal potential and the ion current at zero voltage, (b) cation transference number, and (c) the maximum power generation and energy conversion efficiency for a

SE- PI membrane having parallel (PLNP) and network (NWNP) porous structures. The results correspond to a KCl solution with the concentration ratio 1 M|10 mM. The inset in (b) gives a schematic representation of the PLNP and NWNP membranes.

We consider now the effect of divalent cations on the performance of the SE-PI membrane with 8×10^8 pores cm^{-2} (Figure 7). To this end, we introduce first the asymmetric KCl electrolyte condition $C_H/C_L = 1000$ (1 M|1 mM) and obtain the values $V_{rev} = 122$ mV and $I_0 = -7.0$ µA. The membrane performance is slightly affected when C_L is replaced with 1 mM $CaCl_2$ while C_H is kept constant to 1 M KCl. Also, I_0 is slightly increased from −7.0 µA to −8.3 µA, while V_{rev} is dramatically reduced from 122 mV to 33 mV, as shown in Figure 7(a). A decrease in t_+ from 0.87 to 0.6 is also observed, indicating the significant loss of membrane selectivity, as shown in Figure 7(b). As a consequence, dramatic decreases in P_{max} and η_{max} are obtained (Figure 7c). The performance of the membrane is severely affected when C_H = 1 M $CaCl_2$ and C_L = 1 mM KCl. In this case, the values of I_0 and V_{rev} are almost negligible, *i.e.*, −0.4 µA and 9 mV, respectively. The power P_{max} is close to zero and η_{max} is also negligible compared with the former cases. The cation transference number ~0.5 suggests the loss of membrane selectivity. In agreement with these results, we have recently reported that the soft-etched nanopores hindered significantly the divalent flow across the membrane [17, 18]. However, for the case of the $CaCl_2$ concentration difference C_H = 1 M and C_L = 1 mM, the SE- PI membrane generated V_{rev} and I_o values of −28 mV and +2.7 µA, respectively (Figure 7a). These signs of V_{rev} and I_0 are reversed compared to the above cases, suggesting thus that the membrane surface charge switches from negative to positive due to the binding of Ca^{2+} to the negative deprotonated carboxylate moieties [41]. In agreement with this switching, the transference number $t_- = 0.4$ suggests also a slight anion-selective behavior of the membrane (Figure 7b). Note here that the interaction between the ionic permeant charge and the membrane effective charge dictates the membrane selectivity [42, 43].

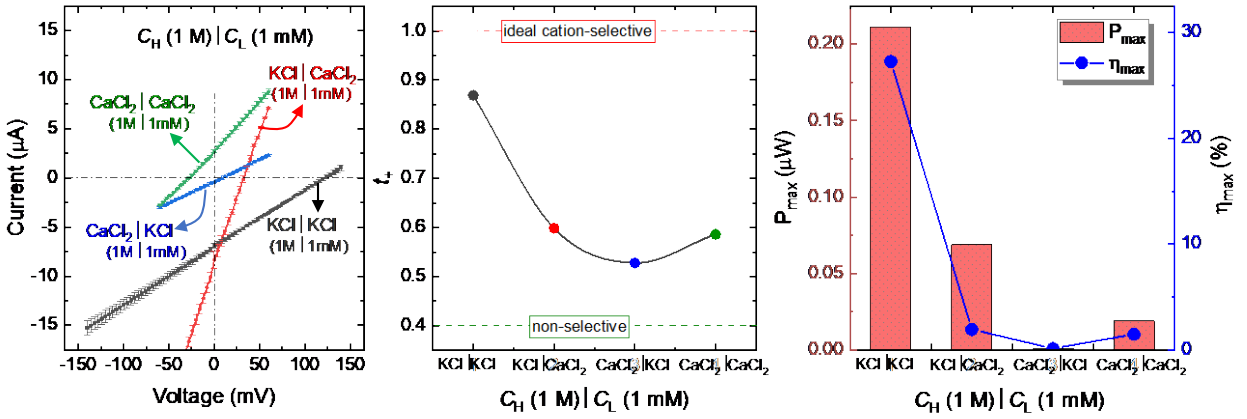

Figure 7. (a) The *I–V* characteristics, (b) cation transference number, and (c) maximum power generation and energy conversion efficiency of a membrane with 8×10^8 pores cm^{-2}. The results correspond to the concentration ratio 1 M | 1 mM and different asymmetric electrolyte solutions.

4. Conclusions

In summary, we have described the behavior of the SE-PI membranes in energy harvesting under a salinity gradient. The nanopore surface is negatively charged and hence favor cation selectivity [17, 18], as evidenced from the transference number [44]. The membrane performance is studied in terms of V_{rev}, I_0 and P_{max} for a wide range of concentration differences. Maximum values for the reversal potential, the maximum power generation, and energy conversion efficiency were 123 mV, 0.45 μW, and 40% for a membrane exposed area of ~1 cm^2. A significant reduction in V_{rev} was noticed for membrane samples with ion fluences higher than 4×10^9 ions cm^{-2}. Moreover, the power generation increased with the concentration ratio and ion fluences up to 4×10^9 ions cm^{-2}. A further fluence increase gave a decrease in power generation due to the overlapping of nanopores and the effect of the external diffusion boundary layers flanking the membrane. Although we initially fixed C_H/C_L = 100 (1 M|10 mM), the diffusion of the ions down this high concentration gradient should eventually give a lower effective value of C_H/C_L because of the time dependent concentration polarization developed at the two diffusion boundary layers flanking the membrane

at low ionic concentrations and high membrane pore density. The use of divalent cations at high concentration was detrimental for the membrane performance because the soft-etched nanopores hindered the cation flow. The soft-etched SE-PI membranes hold the V_{rev} values for several days.

Acknowledgements

S.N., M.A., M.H.A.H. and W.E. acknowledge the support from the LOEWE project iNAPO, Hessen State Ministry of Higher Education, Research and the Arts, Germany. P.R., J. C., and S. M. acknowledge the funding from project PGC2018-097359-B-I00, Ministry of Science and Innovation and FEDER. The authors are thankful to Prof. C. Trautmann and Dr. M. E. Toimil Molares (GSI, Material Research Department) for their support with the heavy ion irradiation experiments. The heavy ion irradiation is based on a UMAT experiment, which was performed at the X0-beamline of the UNILAC at the GSI Helmholtzzentrum für Schwerionenforschung, Darmstadt (Germany) in the frame of FAIR Phase-0.

References

[1] K. Kwon, S.J. Lee, L. Li, C. Han, D. Kim, Energy harvesting system using reverse electrodialysis with nanoporous polycarbonate track-etch membranes, Int. J. Energy Res., 38 (2014) 530-537. https://doi.org/10.1002/er.3111.

[2] O. Schaetzle, C.J.N. Buisman, Salinity Gradient Energy: Current State and New Trends, Engineering, 1 (2015) 164-166. https://doi.org/10.15302/J-ENG-2015046.

[3] F. Goldschmidtboeing, P. Woias, Characterization of different beam shapes for piezoelectric energy harvesting, J. Micromechanics Microengineering, 18 (2008) 104013. https://doi.org/10.1088/0960-1317/18/10/104013.

[4] T. Huesgen, J. Ruhhammer, G. Biancuzzi, P. Woias, Detailed study of a micro heat engine for thermal energy harvesting, J. Micromechanics Microengineering, 20 (2010) 104004. https://doi.org/10.1088/0960-1317/20/10/104004.

[5] F.H.J. van der Heyden, D.J. Bonthuis, D. Stein, C. Meyer, C. Dekker, Electrokinetic Energy Conversion Efficiency in Nanofluidic Channels, Nano Lett., 6 (2006) 2232-2237. https://doi.org/10.1021/nl061524l.

[6] D.-K. Kim, C. Duan, Y.-F. Chen, A. Majumdar, Power generation from concentration gradient by reverse electrodialysis in ion-selective nanochannels, Microfluid. Nanofluid., 9 (2010) 1215-1224. https://doi.org/10.1007/s10404-010-0641-0.

[7] L. Zhao, Y. Yang, Toward Small-Scale Wind Energy Harvesting: Design, Enhancement, Performance Comparison, and Applicability, Shock Vib., 2017 (2017) 3585972. https://doi.org/10.1155/2017/3585972.

[8] W. Guo, L. Cao, J. Xia, F.-Q. Nie, W. Ma, J. Xue, Y. Song, D. Zhu, Y. Wang, L. Jiang, Energy Harvesting with Single-Ion-Selective Nanopores: A Concentration-Gradient-Driven Nanofluidic Power Source, Adv. Funct. Mater., 20 (2010) 1339-1344. https://doi.org/10.1002/adfm.200902312.

[9] D.A. Vermaas, J. Veerman, N.Y. Yip, M. Elimelech, M. Saakes, K. Nijmeijer, High Efficiency in Energy Generation from Salinity Gradients with Reverse Electrodialysis, ACS Sustain. Chem. Eng., 1 (2013) 1295-1302. https://doi.org/10.1021/sc400150w.

[10] T. Ma, E. Balanzat, J.-M. Janot, S. Balme, Nanopore Functionalized by Highly Charged Hydrogels for Osmotic Energy Harvesting, ACS Appl. Mater. Interfaces, 11 (2019) 12578-12585. https://doi.org/10.1021/acsami.9b01768.

[11] J.G. Hong, B. Zhang, S. Glabman, N. Uzal, X. Dou, H. Zhang, X. Wei, Y. Chen, Potential ion exchange membranes and system performance in reverse electrodialysis for power generation: A review, J. Membr. Sci., 486 (2015) 71-88. https://doi.org/10.1016/j.memsci.2015.02.039.

[12] G. Laucirica, A.G. Albesa, M.E. Toimil-Molares, C. Trautmann, W.A. Marmisollé, O. Azzaroni, Shape matters: Enhanced osmotic energy harvesting in bullet-shaped nanochannels, Nano Energy, 71 (2020) 104612. https://doi.org/10.1016/j.nanoen.2020.104612.

[13] M. Tagliazucchi, I. Szleifer, 2 - Theoretical Basis for Structure and Transport in Nanopores and Nanochannels, in: M. Tagliazucchi, I. Szleifer (Eds.) Chemically Modified Nanopores and Nanochannels, William Andrew Publishing, Boston, 2017, pp. 27-60.

[14] S. Ma, Y. Wang, C. Liu, Q. Xu, Z. Min, Preparation and characterization of nanoporous polyimide membrane by the template method as low-k dielectric material, Polym. Adv. Technol., 27 (2016) 414-418. https://doi.org/10.1002/pat.3686.

[15] S. Hirai, P. Phanthong, T. Wakabayashi, S. Yao, Fabrication of Porous Polyimide Membrane with Through-Hole via Multiple Solvent Displacement Method, ChemistryOpen, 10 (2021) 352-359. https://doi.org/10.1002/open.202000299.

[16] W. Kim, M.-K. Lee, Fabrication of a porous polyimide membrane using a silicon nanowire array as a template, Mater. Lett., 63 (2009) 933-936. https://doi.org/10.1016/j.matlet.2009.01.060.

[17] K. Froehlich, S. Nasir, M. Ali, P. Ramirez, J. Cervera, S. Mafe, W. Ensinger, Fabrication of soft-etched nanoporous polyimide membranes for ionic conduction and discrimination, J. Membr. Sci., 617 (2021) 118633. https://doi.org/10.1016/j.memsci.2020.118633.

[18] M. Ali, S. Nasir, K. Froehlich, P. Ramirez, J. Cervera, S. Mafe, W. Ensinger, Size-Based Cationic Molecular Sieving through Solid-State Nanochannels, Adv. Mater. Interfaces, 8 (2021) 2001766. https://doi.org/10.1002/admi.202001766.
[19] S. Nasir, M. Ali, P. Ramirez, K. Froehlich, J. Cervera, S. Mafe, W. Ensinger, Ionic conduction through single-pore and multipore polymer membranes in aprotic organic electrolytes, J. Membr. Sci., 635 (2021) 119505. https://doi.org/10.1016/j.memsci.2021.119505.
[20] M. Ali, B. Schiedt, K. Healy, R. Neumann, W. Ensinger, Modifying the surface charge of single track-etched conical nanopores in polyimide, Nanotechnology, 19 (2008) 085713. https://doi.org/10.1088/0957-4484/19/8/085713
[21] Z. Siwy, D. Dobrev, R. Neumann, C. Trautmann, K. Voss, Electro-responsive asymmetric nanopores in polyimide with stable ion-current signal, Appl. Phys., 76 (2003) 781-785. https://doi.org/10.1007/s00339-002-0982-7.
[22] P. Wang, M. Wang, F. Liu, S. Ding, X. Wang, G. Du, J. Liu, P. Apel, P. Kluth, C. Trautmann, Y. Wang, Ultrafast ion sieving using nanoporous polymeric membranes, Nat. Commun., 9 (2018) 569. https://doi.org/10.1038/s41467-018-02941-6.
[23] J. Lu, H. Zhang, J. Hou, X. Li, X. Hu, Y. Hu, C.D. Easton, Q. Li, C. Sun, A.W. Thornton, M.R. Hill, X. Zhang, G. Jiang, J.Z. Liu, A.J. Hill, B.D. Freeman, L. Jiang, H. Wang, Efficient metal ion sieving in rectifying subnanochannels enabled by metal–organic frameworks, Nat. Mater., 19 (2020) 767-774. https://doi.org/10.1038/s41563-020-0634-7.
[24] Z. Siwy, I.D. Kosinska, A. Fulinski, C.R. Martin, Asymmetric diffusion through synthetic nanopores, Phys. Rev. Lett., 94 (2005) 048102. https://doi.org/10.1103/PhysRevLett.94.048102.

[25] P. Ramirez, J. Cervera, V. Gomez, M. Ali, S. Nasir, W. Ensinger, S. Mafe, Membrane potential of single asymmetric nanopores: Divalent cations and salt mixtures, J. Membr. Sci., 573 (2019) 579-587. https://doi.org/10.1016/j.memsci.2018.12.043.
[26] A.H. Galama, J.W. Post, H.V.M. Hamelers, V.V. Nikonenko, P.M. Biesheuvel, On the Origin of the Membrane Potential Arising Across Densely Charged Ion Exchange Membranes: How Well Does the Teorell-Meyer-Sievers Theory Work?, J. Membr.Sci. Res., 2 (2016) 128-140. https://doi.org/10.22079/jmsr.2016.20311.
[27] L.-H. Yeh, C. Hughes, Z. Zeng, S. Qian, Tuning Ion Transport and Selectivity by a Salt Gradient in a Charged Nanopore, Anal. Chem., 86 (2014) 2681-2686. https://doi.org/10.1021/ac4040136.
[28] Y. Lanteri, A. Szymczyk, P. Fievet, Membrane Potential in Multi-Ionic Mixtures, J. Phys. Chem. B, 113 (2009) 9197-9204. https://doi.org/10.1021/jp901110c.
[29] S. Balme, T. Ma, E. Balanzat, J.-M. Janot, Large osmotic energy harvesting from functionalized conical nanopore suitable for membrane applications, J. Membr. Sci., 544 (2017) 18-24. https://doi.org/10.1016/j.memsci.2017.09.008.
[30] W.J. Hamer, Y.C. Wu, Osmotic Coefficients and Mean Activity Coefficients of Uni-univalent Electrolytes in Water at 25°C, J. Phys. Chem. Ref. Data 1(1972) 1047-1100. https://doi.org/10.1063/1.3253108.
[31] B.R. Staples, R.L. Nuttall, The activity and osmotic coefficients of aqueous calcium chloride at 298.15 K, J. Phys. Chem. Ref. Data, 6 (1977) 385-408. https://doi.org/10.1063/1.555551.
[32] F. Xiao, D. Ji, H. Li, J. Tang, Y. Feng, L. Ding, L. Cao, N. Li, L. Jiang, W. Guo, A general strategy to simulate osmotic energy conversion in multi-pore nanofluidic systems, Mater. Chem. Front., 2 (2018) 935-941. https://doi.org/10.1039/C8QM00031J.
[33] J. Gao, X. Liu, Y. Jiang, L. Ding, L. Jiang, W. Guo, Understanding the Giant Gap between Single-Pore- and Membrane-Based Nanofluidic Osmotic Power Generators, Small, 15 (2019) 1804279. https://doi.org/10.1002/smll.201804279.
[34] Z. Zhang, L. Wen, L. Jiang, Nanofluidics for osmotic energy conversion, Nat. Rev. Mater., 6 (2021) 622-639. DOI 10.1038/s41578-021-00300-4. https://doi.org/10.1021/nl2005516.
[35] L. Wang, Z. Wang, S.K. Patel, S. Lin, M. Elimelech, Nanopore-Based Power Generation from Salinity Gradient: Why It Is Not Viable, ACS Nano, 15 (2021) 4093-4107. https://doi.org/10.1021/acsnano.0c08628.

[36] M. Rauber, I. Alber, S. Müller, R. Neumann, O. Picht, C. Roth, A. Schökel, M.E. Toimil-Molares, W. Ensinger, Highly-Ordered Supportless Three-Dimensional Nanowire Networks with Tunable Complexity and Interwire Connectivity for Device Integration, Nano Lett., 11 (2011) 2304-2310. https://doi.org/10.1021/nl2005516.
[37] G. Yang, D. Liu, C. Chen, Y. Qian, Y. Su, S. Qin, L. Zhang, X. Wang, L. Sun, W. Lei, Stable Ti3C2Tx MXene–Boron Nitride Membranes with Low Internal Resistance for Enhanced Salinity Gradient Energy Harvesting, ACS Nano, 15 (2021) 6594-6603. https://doi.org/10.1021/acsnano.0c09845.
[38] Y. Wu, W. Xin, X.-Y. Kong, J. Chen, Y. Qian, Y. Sun, X. Zhao, W. Chen, L. Jiang, L. Wen, Enhanced ion transport by graphene oxide/cellulose nanofibers assembled membranes for high-performance osmotic energy harvesting, Mater. Horiz., 7 (2020) 2702-2709. https://doi.org/10.1039/D0MH00979B.
[39] P. Ramírez, S. Mafé, J.A. Manzanares, J. Pellicer, Membrane potential of bipolar membranes, J. Electroanal. Chem., 404 (1996) 187-193. https://doi.org/10.1016/0022-0728(95)04378-0.
[40] S. Mafé, V.M. Aguilella, J. Pellicer, Film control and membrane control in charged membranes, J. Membr. Sci., 36 (1988) 497-509. https://doi.org/10.1016/0376-7388(88)80039-5.

[41] M. Ali, S. Nasir, P. Ramirez, J. Cervera, S. Mafe, W. Ensinger, Calcium Binding and Ionic Conduction in Single Conical Nanopores with Polyacid Chains: Model and Experiments, ACS Nano, 6 (2012) 9247-9257. https://doi.org/10.1021/nn303669g.
[42] A.V. Sokirko, P. Ramírez, J.A. Manzanares, S. Mafé, Modeling of Forward and Reverse Bias Conditions in Bipolar Membranes, Ber. Bunsenges. phys. Chem., 97 (1993) 1040-1048. https://doi.org/10.1002/bbpc.19930970814.
[43] T. Jimbo, P. Ramirez, A. Tanioka, S. Mafe, N. Minoura, Passive transport of ionic drugs through membranes with pH-dependent fixed charges, J. Colloid Interface Sci., 225 (2000) 447-454. https://doi.org/10.1006/jcis.2000.6779
[44] J.-P. Hsu, S.-C. Lin, C.-Y. Lin, S. Tseng, Power generation by a pH-regulated conical nanopore through reverse electrodialysis, J. Power Sources, 366 (2017) 169-177. https://doi.org/10.1016/j.jpowsour.2017.09.022